

THE LOCAL STAR FORMATION RATE SURFACE DENSITY AND METALLICITY RELATION FOR STAR-FORMING GALAXIES

BERZAF BERHANE TEKLU ^{1,2} YULONG GAO ^{1,2,3} XU KONG ^{1,2} ZESEN LIN ^{1,2} AND ZHIXIONG LIANG ^{1,2}

¹CAS Key Laboratory for Research in Galaxies and Cosmology, Department of Astronomy, University of Science and Technology of China, Hefei 230026, China

²School of Astronomy and Space Science, University of Science and Technology of China, Hefei 230026, China

³Institute of Astronomy, The University of Tokyo, Osawa 2-21-1, Mitaka, Tokyo 181-0015, Japan

Submitted to ApJ

ABSTRACT

We study the relations between gas-phase metallicity (Z), local stellar mass surface density (Σ_*), and the local star formation surface density (Σ_{SFR}) in a sample of 1120 star-forming galaxies from the MaNGA survey. At fixed Σ_* the local metallicity increases as decreasing of Σ_{SFR} or vice versa for metallicity calibrators of N2 and O3N2. Alternatively, at fixed Σ_{SFR} metallicity increases as increasing of Σ_* , but at high mass region, the trend is flatter. However, the dependence of metallicity on Σ_{SFR} is nearly disappeared for N2O2 and N2S2 calibrators. We investigate the local metallicity against Σ_{SFR} with different metallicity calibrators, and find negative/positive correlations depending on the choice of the calibrator. We demonstrate that the O32 ratio (or ionization parameter) is probably dependent on star formation rate at fixed local stellar mass surface density. Additional, the shape of $\Sigma_* - Z - \Sigma_{\text{SFR}}$ (FMR) depends on metallicity calibrator and stellar mass range. Since the large discrepancy between the empirical fitting-based (N2, O3N2) to electronic temperature metallicity and the photoionization model-dependent (N2O2, N2S2) metallicity calibrations, we conclude that the selection of metallicity calibration affects the existence of FMR on Σ_{SFR} .

Keywords: galaxies: abundances - galaxies: evolution - galaxies: local - galaxies: ISM

1. INTRODUCTION

Understanding the physical process of the interstellar medium (ISM) is a key for determining a complete picture of galaxy formation and evolution. In particular, metallicity over galaxies is one of the physical quantities to implement a hint regarding evolution. The metallicity could produce insights into regulating galaxy outflow properties (Finlator & Davé 2008; Lilly et al. 2013; Belfiore et al. 2016). The enrichment gas outflow and inflow decreased the gas-phase abundance inside a galaxy. The inflows dilute the metal content, while the outflows remove metals from the ISM. The galaxy metallicity will reduce if the outflow gas is enriching beyond the current ISM, either through the direct escape of metal-rich ejection from the supernova explosion (SNe) or through galactic winds with enriched metals.

The relation of mass-metallicity (MZR) was established by Lequeux et al. (1979), which indicates that the metallicity of

galaxy increases as increasing of the stellar mass, this recognizes that the galactic outflows controlling the metal content of the interstellar medium. Since it was presented observationally with the aid of Tremonti et al. (2004), who determined a tight relation spanning upon three orders of magnitude within the mass and a factor concerning about 0.1 dex into metallicity, using a large sample of star-forming galaxies from Sloan Digital Sky Survey (SDSS). Moreover, the MZR presents an entirely similar shape impartially concerning the oxygen abundance calibrator, including a clear trend for $M_* < 10^{10} M_\odot$, then pulling down to the asymptotic value for higher stellar masses (e.g., Kewley & Ellison 2008).

In particular, Ellison et al. (2008) had already shown the dependence of MZR on star formation rate. Alternatively, Lara-López et al. (2010) and Mannucci et al. (2010) suggested the correlation between metallicity and star formation rate (SFR), observing that at a fixed mass, the lower metallicity galaxy shows higher SFR. However, both of the SFR and metallicity increase with increasing of galaxy stellar mass. Besides, numerous studies confirmed the M-Z-SFR (FMR) relation (e.g., Mannucci et al. 2010; Hunt et al. 2012; Yates

et al. 2012; Andrews & Martini 2013; Salim et al. 2014; Wu et al. 2016; Sánchez Almeida et al. 2018; Sánchez Almeida & Sánchez-Menguiano 2019).

Furthermore, several studies also questioned the presence of FMR relation. Sánchez et al. (2013) obtained H II regions from the CALIFA data set (Sánchez et al. 2012) but did not find the secondary relation with SFR. Moran et al. (2012) had shown that their data does not demonstrate this secondary relation; however, they suggested a secondary relationship to the gas fraction. Furthermore, Rosales-Ortega et al. (2012) found a correlation with specific SFR (sSFR) based on the equivalent width (EW) of H α . The local MZR does not exhibit a secondary relation yet maintaining the primary link between stellar mass and SFR. Kashino et al. (2016) revealed that they could not determine the secondary dependence between SFR and MZR presented by Mannucci et al. (2010) for a single metallicity calibrator. More recently, Barrera-Ballesteros et al. (2017) used different metallicity calibrators; at any of the calibrations, they have not found a robust secondary trend of MZR with neither SFR nor sSFR. However, in a recent review about the FMR, Cresci et al. (2019) found the presence of FMR at fixed stellar mass by reanalyzing the data of CALIFA and SDSS-IV MaNGA.

In addition, the mass-metallicity relation is also mainly important for stellar evolution. Many studies (Moran et al. 2012; Rosales-Ortega et al. 2012; Sánchez et al. 2013; Gao et al. 2018) explored the correlation of the local metallicity and the local stellar mass density for local star-forming galaxies using the GASS survey (Saintonge et al. 2011), CALIFA survey (Sánchez et al. 2012), and the MaNGA survey (Bundy et al. 2015), respectively. Those authors confirmed the existence of correlation between local metallicity and local surface mass density. Alternatively, they noticed that H II regions with higher mass surface density are metal-rich than lower densities.

Moreover, the relation between SFR and ionization parameter are not well understood. Kewley & Dopita (2002) defined the ionization parameter using two-line ratio [O III]/[O II]. Lately, Nakajima & Ouchi (2014) presented a correlation between the ionization parameter and the global physical properties of galaxies and found that higher ionization parameters are determined in much less massive galaxies with low metallicity. In addition, the anti-correlation between the ionization parameter and metallicity of H II region was also presented by Dopita et al. (2006). In particular, Kaasinen et al. (2018) find that higher ionization parameters toward higher sSFRs for their star-forming galaxies. High ionization parameter has been proposed as the result of high SFRs, contributing to a larger reservoir of ionizing photons (e.g., Kewley et al. 2013).

Although, significant studies about the local MZR and FMR did not take the sensitivity of ionization parameter into

account the metallicity and star formation rate. In this study, we perform a large spatially resolved samples from MaNGA IFU survey to investigate the relation of local stellar surface density, metallicity, and local star formation rate surface density ($\Sigma_* - Z - \Sigma_{\text{SFR}}$). We also take a look at the effects of the ionization parameter with different metallicity diagnostics.

The paper is organized as follows. In Section 2, we demonstrate the sample selection for star-forming galaxies from the MaNGA survey, fitting process, determination of the gas-phase oxygen abundances, stellar mass surface densities, and other physical parameters. In Section 3, we investigate the distribution and relation of $\Sigma_* - Z - \Sigma_{\text{SFR}}$, and the dependence of the ionization parameter with metallicity. We discuss the implication of our results of the fundamental metallicity relation (FMR) and $\Sigma_{\text{SFR}} - Z$ in Section 4. Finally, we summarize our results in Section 5. Throughout this paper, we adopt a flat Λ CDM cosmology with $\Omega_\Lambda = 0.7$, $\Omega_m = 0.3$, and $H_0 = 70 \text{ km s}^{-1} \text{ Mpc}^{-1}$.

2. DATA

2.1. MaNGA Overview

The MaNGA survey is to examine 10,000 galaxies using an integral field spectroscopy unit (IFU), across 2700 deg^2 at local universe $z \sim 0.03$ (Bundy et al. 2015). The wavelength ranges from 3600 to 10300 Å with spectral resolution $R \sim 1400$ to 2600. The standard effective spatial resolution of the extracted data cubes can be used to illustrate by Gaussian with an FWHM $\sim 2.5''$, and the spaxel size of released datacubes is $0.5''$. The MaNGA IFU includes 29 fiber bundles in the SDSS field of view. A further detailed description of MaNGA instrument structure can be found in Drory et al. (2015).

In this study, we extract the MaNGA data from SDSS-IV Data Release 14 (DR14)¹ (Abolfathi et al. 2018) as the initial sample that contains 2812 galaxies.

2.2. Spectral Fitting and Emission-line Measurements

Firstly, we correct the Galactic extinction by applying the color excess $E(B - V)$ using a map of Milky Way (Schlegel et al. 1998). For this study we use the public STARLIGHT spectral fitting code (Cid Fernandes et al. 2005) to fit the observational continuum spectra with a series of single stellar population (SSP) models from Bruzual & Charlot (2003), assuming a Chabrier (2003) initial mass function (IMF) and adopting the attenuation law of Calzetti et al. (2000).

The fluxes of strong emission lines (e.g., [O II] λ 3727, H β , [O III] λ 4959, 5007, H α , [N II] λ 6583 and [S II] λ 6717,6731) are fitted with the Gaussian profiles by applying an IDL package MPFIT (Markwardt et al. 2009).

¹ <http://www.sdss.org/dr14/manga/manga-data/catalogs>

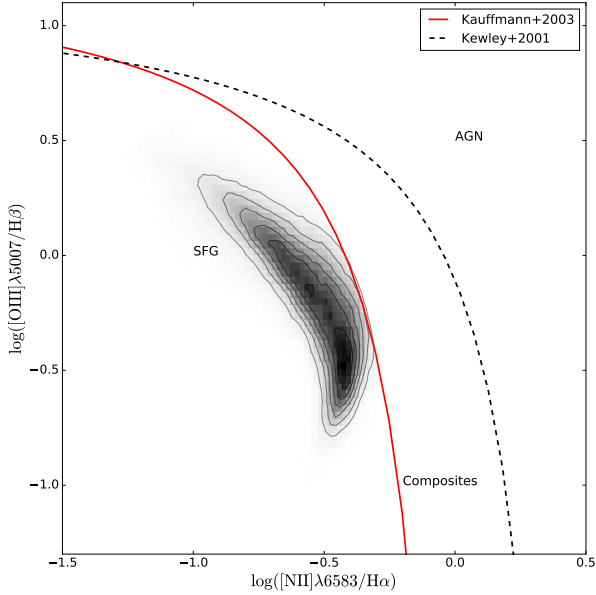


Figure 1. The BPT diagram for spaxels of star-forming galaxies in our sample. The grayscale histogram exhibit the observation number density. The red solid and black dashed lines represent the demarcation curves between SFGs and AGNs characterized by [Kauffmann et al. \(2003\)](#) and [Kewley et al. \(2001\)](#), respectively.

Following the method of [Ly et al. \(2014\)](#), we measure the signal-to-noise ratios (S/N) of these emission lines. Using Balmer decrement and assuming [Calzetti et al. \(2000\)](#) attenuation law, we correct the interstellar reddening. We presume the intrinsic flux ratio $(H\alpha/H\beta)_0 = 2.86$ under the case-B recombination.

2.3. Sample Selection

Our parent sample has 2812 galaxies from SDSS DR14, and we suppose to use the benchmark of $NUV - r < 4$ to select star-forming galaxies ([Li et al. 2015](#)), then 1120 galaxies are selected. Our main goal is to select star-forming regions, we appear the spaxels have signal to noise ratio $S/N(H\alpha) > 5$, $S/N(H\beta) > 5$, $S/N([O III]\lambda 3727) > 5$, $S/N([O III]\lambda\lambda 4959, 5007) > 5$, $S/N([N II]\lambda 6583) > 3$, with continuum S/N greater than 3 and the equivalent width of $H\alpha$ greater than 10 \AA . We use the [Kauffmann et al. \(2003\)](#) boundary line in the BPT diagram ([Baldwin et al. 1981](#); [Kewley et al. 2001](#); [Kauffmann et al. 2003](#)) to exclude the spaxels affected by the active galactic nucleus (AGNs).

Figure 1 illustrates the BPT diagram of about 740,000 spaxels. The grayscale exhibits the spaxel number density. As shown, our final sample of spaxels located in the star forming region.

2.4. Determinations of Metallicity, Star Formation Rate Surface Density, and Stellar Mass Surface Density

Determination of accurate oxygen abundance is more reliable using the electronic temperature or direct method, which can be obtained from the ratio of auroral to nebular intensity lines, such as $[O III]\lambda 4363/[O III]\lambda 5007$. Getting the oxygen abundance using the direct method is challengeable for higher metallicity because $[O III]\lambda 4363$ becomes fainter. In this study, we will adopt four metallicity calibrations based on strong lines.

I). The N2O2 calibrator is a more reliable estimator for local galaxies because of the spectral wavelength coverage. For nearby galaxies, we can get the lines of $[O II]\lambda 3727$ and $[N II]\lambda 6583$, but for the higher redshift, it is challengeable to observe those lines. Additional, the ratio of $[N II]$ and $[O II]$ is less affected by the ionization distribution, thus the N2O2 can be an oxygen abundance indicator. The calibrated metallicity using the relation in [Kewley & Dopita \(2002\)](#) is given by:

$$12 + \log(O/H) = \log(1.54020 + 1.26602 \times N2O2 + 0.167977 \times N2O2^2) + 8.93, \quad (1)$$

where $N2O2 \equiv \log([(N II)\lambda 6583]/([O II]\lambda\lambda 3727, 3729))$, with estimated uncertainty of 0.04 dex.

II). O3N2: This index is commonly known as that it depends on strong emission line flux ($H\alpha$, $H\beta$, $[O III]\lambda 5007$, $[N II]\lambda 6583$) to diagnose oxygen abundances in the literature. The diagnostic of O3N2 index ([Alloin et al. 1979](#)) is characterized by

$$O3N2 \equiv \log\left(\frac{[O III]\lambda 5007}{H\beta} \times \frac{H\alpha}{[N II]\lambda 6583}\right). \quad (2)$$

[Pettini & Pagel \(2004\)](#) recalibrate O3N2 diagnostic with T_e based metallicity for H II region samples. Later, [Marino et al. \(2013\)](#) improved the O3N2 calibration with a large sample of H II regions. Here we use the modified O3N2 calibration by [Marino et al. \(2013\)](#), which is given by

$$12 + \log(O/H) = 8.505 - 0.221 \times O3N2. \quad (3)$$

III). N2: [Storchi-Bergmann et al. \(1994\)](#) initially suggested the N2 index as a calibrator because the N2 index strongly correlated with abundance. The diagnostic N2 index ([Storchi-Bergmann et al. 1994](#); [Raimann et al. 2000](#)) is described as

$$N2 \equiv \log([N II]\lambda 6583/H\alpha). \quad (4)$$

Hence, N2 calibrated metallicity is determined by [Marino et al. \(2013\)](#) and expressed as

$$12 + \log(O/H) = 8.667 + 0.455 \times N2. \quad (5)$$

IV). N2S2 index: The $[N II]\lambda 6583/[S II]\lambda\lambda 6717, 6731$ diagnostic is sensitive to metallicity and weakly dependent on the ionization parameter. The N2S2 index is defined as:

$$N2S2 \equiv \log\left(\frac{[N II]\lambda 6583}{[S II]\lambda\lambda 6717, 6731}\right), \quad (6)$$

and the metallicity calibration relation using the N2 and N2S2 from [Dopita et al. \(2016\)](#) is given as

$$12 + \log(\text{O}/\text{H}) = 8.77 + \text{N2S2} + 0.264 \times \text{N2}. \quad (7)$$

The global stellar mass M_* and minor-to-major axis ratio (b/a) are extracted from the NSA catalog ² ([Blanton et al. 2005](#), [Blanton et al. 2011](#)). Following the method of [Barrera-Ballesteros et al. \(2016\)](#), we generate the local stellar mass surface density Σ_* . We divide the surface mass density in each spaxel from the output results of STARLIGHT by its corresponding physical area and then correct the inclination using the b/a .

We use the dust-corrected $\text{H}\alpha$ emission-line luminosity to determine the star formation rate for each spaxel, using the formula from [Kennicutt \(1998\)](#) and assuming a [Chabrier \(2003\)](#) IMF.

3. RESULT

In this section, we utilize the dependence of $\Sigma_* - Z$ relation as a function of the local Σ_{SFR} . Moreover, we explore the dependence of the $\Sigma_* - Z$ relation on star formation rate surface density and the ratio of $[\text{O III}]\lambda 5007/[\text{O II}]\lambda 3727$.

3.1. The Dependence of the $\Sigma_* - Z$ Relation on Star Formation Rate Surface Density

In [Gao et al. \(2018\)](#), we reported the relationship between the local stellar mass surface density and gas metallicity and found similar relations with [Rosales-Ortega et al. \(2012\)](#) and [Sánchez et al. \(2013\)](#). As proposed in these results, it is necessary to check if the local $\Sigma_* - Z$ relationships have a secondary relationship with local Σ_{SFR} .

As mentioned above, we investigate the dependence of local metallicity and the local stellar mass surface density Σ_* as a function of local star formation rate surface density ($\Sigma_* - Z - \Sigma_{\text{SFR}}$) relation for our samples in [Figure 2](#). We separate our sample into five different bins based on local star formation rate surface density, and each panel shows different metallicity indicators. The bins are ranging from lower to higher Σ_{SFR} (-3.65 , -2.45 , -2.2 , -2 and -1.65) values. The median values for different star formation ranges are shown as the different color code connected lines.

In the top left and right panels of [Figure 2](#), we present the metallicity derived by N2 and O3N2 indexes as a function of the local stellar mass surface density. As shown in these panels, the metallicity increases with increasing of local stellar mass surface density. Compared to the higher star formation rate surface density region, the lower star formation rate surface density region shows higher metallicity at a fixed Σ_* . In this case, there is a tendency that the star formation rate surface density decreases as the metallicity increases.

The bottom left and right panels of [Figure 2](#), show the metallicity derived with N2O2 and N2S2 indexes, respectively. In these panels, the trend of $\Sigma_* - Z$ is similar to N2 and O3N2, however, not obvious as a function of local Σ_{SFR} . Interestingly, we notice that the Σ_{SFR} does not change with increasing metallicity at fixed Σ_* . In particular, the metallicity increases steeply with local stellar mass surface density, while flatter relation appears at high mass surface density ($\log(\Sigma_*) > 7.8$) for the top two panels. However, the difference in the dependence of local MZR on Σ_{SFR} is attributable to the metallicity calculation method between different diagnostics and calibrations, more detail about this discrepancy can be found in previous studies (e.g., [Pettini & Pagel 2004](#); [Kewley & Ellison 2008](#); [Sánchez et al. 2012](#)). On the other hand, the $\text{H}\alpha$ based estimation of Σ_{SFR} also affects the shape of $\Sigma_* - Z - \Sigma_{\text{SFR}}$. We will show more detail about this reversal relation for those different metallicity indicators in the following sections.

3.2. Star Formation Rate Surface Density and Metallicity ($\Sigma_{\text{SFR}} - Z$) Relation on M_*

In the previous section, we examine the relation between $\Sigma_* - Z$, and Σ_{SFR} . In this section, we aim further to test the dependence of Σ_{SFR} on the local metallicity comparing different metallicity calibrations at fixed stellar mass and local stellar mass surface density. To quantify this relation, for each subsample, we derive the correlation coefficient for checking if it presents any variation with the stellar mass. If the $\Sigma_{\text{SFR}} - Z$ change significantly for each stellar mass bin, maybe the shape of $\Sigma_* - Z$ truly depends on the Σ_{SFR} , as we have shown in the top left and right panels in [Figure 2](#) of [Section 3.1](#).

In [Figure 3](#), we show the distribution of metallicity-star formation rate surface density, at fixed global stellar mass and local stellar mass surface density regardless of [Gao et al. \(2018\)](#). The first column shows the distribution at low mass range of $9.2 < \log(M_*/M_\odot) < 9.6$ and $6.4 < \log(\Sigma_*) < 7.1$ with different metallicity calibrations. Second column represents the intermediate-mass bin $9.6 < \log(M_*/M_\odot) < 10.0$ and $7.1 < \log(\Sigma_*) < 7.8$. The last column indicates the high mass bin $10.0 < \log(M_*/M_\odot) < 10.5$ and $7.8 < \log(\Sigma_*) < 8.5$. In each panel, the solid red line indicates the best-fit liner relation of $\Sigma_{\text{SFR}} - Z$, and the gray contour represents scatter of subsamples.

For low mass bin subsamples, we find a clear and strong anti-correlation between Σ_{SFR} and metallicity, with $r = -0.33$ and $r = -0.38$, for metallicity index N2 and O3N2, respectively. However, for N2O2 and N2S2 metallicity indices, no correlation is found at this mass range. Our results regarding correlation coefficients of different metallicities with bins of stellar mass and local surface mass density are shown in [Table 1](#).

² <http://www.nsatlas.org>

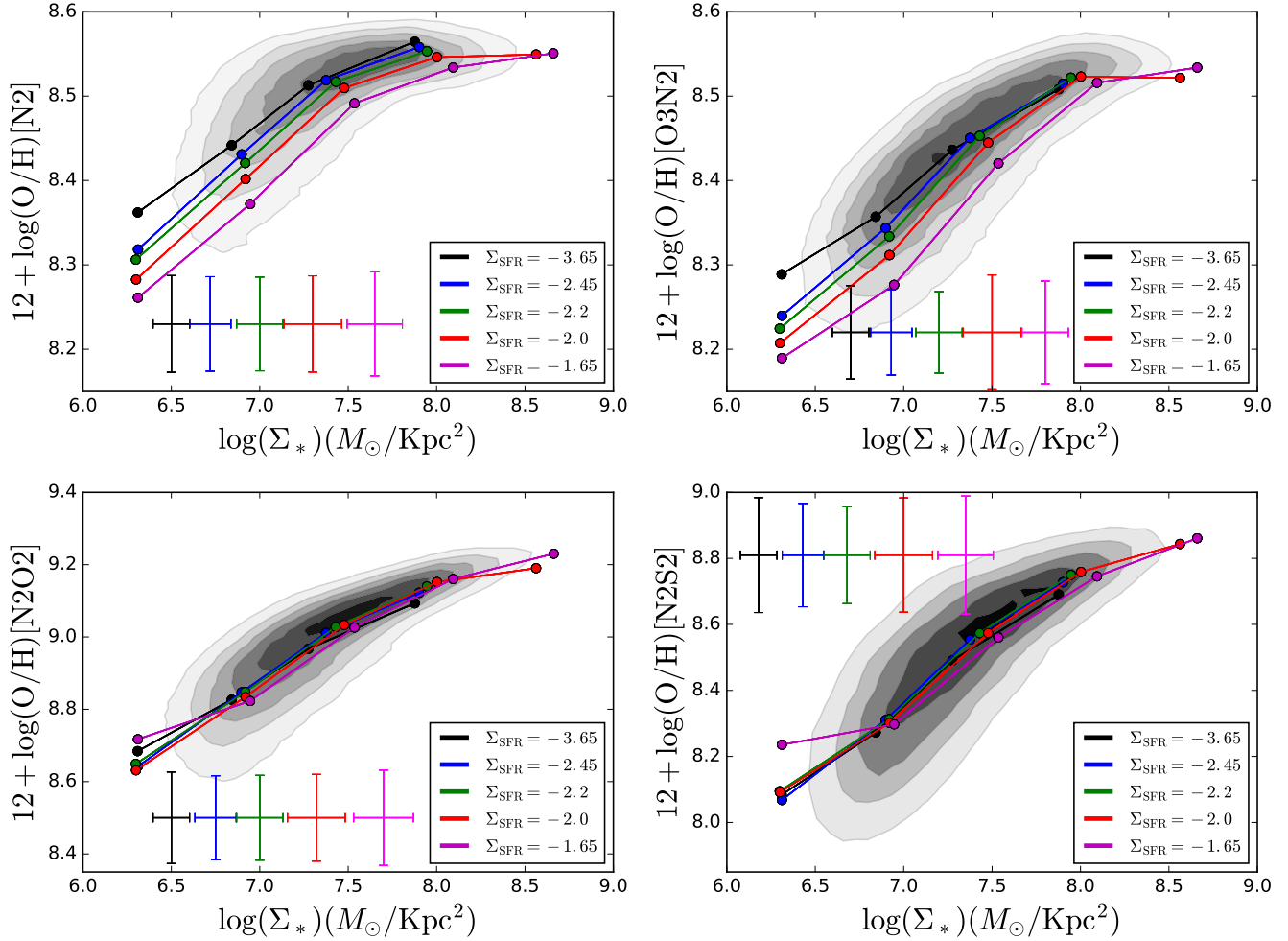


Figure 2. The distribution of metallicity against local stellar mass surface density as regards four different metallicity calibrations, O3N2, N2, N2O2 and N2S2 indexes. We separate our spatially resolved MaNGA samples into five subsamples based on local star formation surface densities (Σ_{SFR}), which are binned as -3.69 , -2.45 , -2.2 , -2 and -1.65 . The left top and right top panels shows the relation between Σ_* – Z based on N2 and O3N2 metallicity indicators, respectively. The bottom left and right panels indicates Σ_* – Z relation using the N2O2 index and N2S2 index, respectively. The color-coded symbols with linked lines indicate the median values for different Σ_{SFR} bins. The error-bars serve as the standard deviation of median values in different bins.

Table 1. Correlation Coefficient (r values) of N2, O3N2, N2O2 and N2S2 Metallicity Indices.

$\log(M_*/M_\odot)$	N2	O3N2	N2O2	N2S2
9.2 – 9.6	-0.33	-0.386	0.009	0.056
9.6 – 10.	-0.256	-0.203	0.132	0.092
10. – 10.5	-0.279	-0.025	0.269	0.127

Notes: We separate out the sample according to global stellar mass and local stellar mass surface density. The mass range of first row is $9.2 < \log(M_*/M_\odot) < 9.6$ and $6.4 < \log(\Sigma_*) < 7.1$. Second row mass bin $9.6 < \log(M_*/M_\odot) < 10.$ and $7.1 < \log(\Sigma_*) < 7.8$. The last row shows the range of $10. < \log(M_*/M_\odot) < 10.5$ and $7.8 < \log(\Sigma_*) < 8.5$.

As shown in Figure 3, the $\Sigma_{\text{SFR}} - Z$ relation at different stellar mass bins shows different slopes for N2, O3N2, N2O2, and N2S2 metallicity calibrators. The trends are slightly similar for those two calibrators of N2 and O3N2. If we focus on the low and intermediate-mass bins, we can see that the $\Sigma_{\text{SFR}} - Z$ slope presents anti-correlation. This trend is consistent with [Sánchez Almeida & Sánchez-Menguiano \(2019\)](#) at stellar mass range $9.2 < \log(M_*/M_\odot) < 9.6$ using O3N2 index. Besides considering the N2 index, at fixed mass, the metallicity decreases with increasing of local Σ_{SFR} .

As we explored, the relations indicate that for higher (lower) stellar mass bins, the correlation is weak (strong) for $\Sigma_{\text{SFR}} - Z$. As we shown, for O3N2 metallicity calibration, at higher stellar mass ($\log(M_*/M_\odot) > 10.$), we find a flat

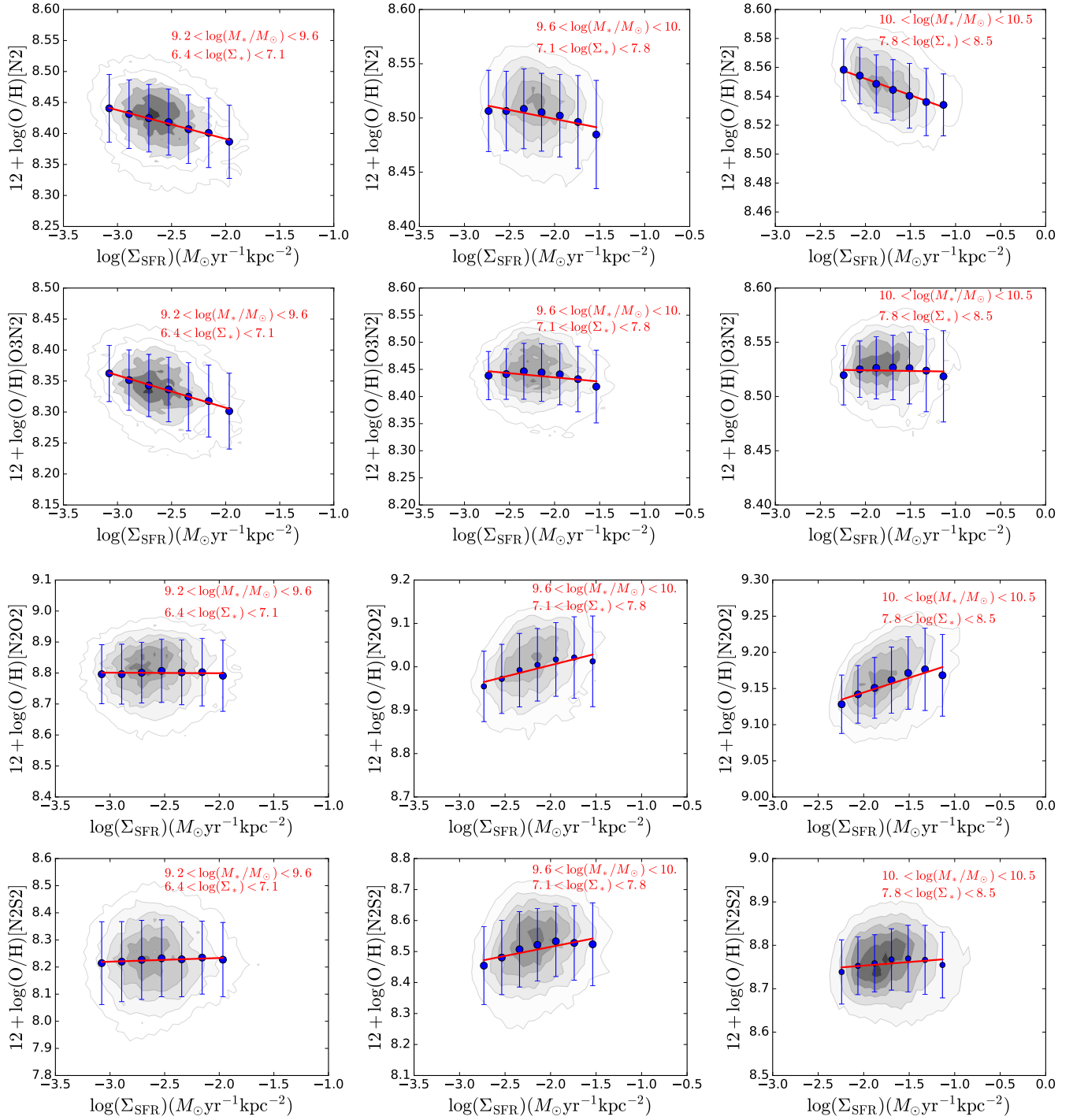


Figure 3. The metallicity distribution in Σ_{SFR} space based on O3N2, N2, N2O2, N2S2 indexes. We separate the plotting range M_* and Σ_* into three bins (M_* : 9.2, 9.6, 10.0, 10.5 & Σ_* : 6.4, 7.1, 7.8, 8.5). The left four rows show the lower mass bin for different metallicity calibration; middle four panels represent the intermediate mass range and the last right four panels show for a higher mass bin for different metallicity calibration, respectively. The contour represents the distribution of $\Sigma_{\text{SFR}} - Z$. The red dashed line in each panel shows the best-fitted $\Sigma_{\text{SFR}} - Z$ relation of subsamples. Blue symbols and error-bars display as the median values and standard deviation, respectively.

ter trend, which is similar to the flat MZR at high mass (e.g., Tremonti et al. 2004; Kewley & Ellison 2008; Zahid et al. 2014). However, Figure 3 shows a positive correlation for N2O2 and N2S2 calibrators, while a negative correlation for N2 index, at high mass region.

Generally, this mixed type of behavior is different from the local MZR and FMR at different stellar mass bin regions for star-forming galaxies reported in other studies. The mixed results on this $\Sigma_{\text{SFR}} - Z$ relations are possibly caused by different metallicity estimation, which have systematic errors on calibration, and the calculation of Σ_{SFR} from strong emission line. The variations among observed behavior are just probably associated along with the methods used to measure the oxygen abundance among different studies.

We expect that the different trends in $\Sigma_{\text{SFR}} - Z$ relations for different stellar mass bins, with four metallicity calibrators, might be caused by the dependence of metallicity on ionization parameter. We will discuss the ionization parameter in the following sections.

3.3. Dependence of $[\text{O III}]\lambda 5007/[\text{O II}]\lambda 3727$ on Metallicity

In this section, we demonstrate the dependence of $[\text{O III}]\lambda 5007/[\text{O II}]\lambda 3727$ on the metallicity. The ratio of O32 is a proxy of the ionization parameter (Dopita et al. 2000; Kewley & Dopita 2002). In Figure 4, we show the metallicity distribution as a function of the O32 ratio with four different calibrators. Different color means different Σ_{SFR} , which are same as Figure 2. The median metallicity is shown for bins of varying Σ_{SFR} . In particular, at a fixed ratio of O32, the metallicity increases with the increasing of Σ_{SFR} .

In Figure 4 we see that the local metallicity is decreasing with the increasing of O32 ratio. As shown in Figure 4, the higher metallicity corresponds with a lower O32 ratio, which is also described by Maier et al. (2004). Dopita et al. (2006) argued that the higher opacity stellar wind causes a strong dependence between chemical abundance and ionization parameter in the surrounding H II region. We investigate that the metallicity calibrator depends on the ionization parameter or the ratio of O32. We expect that the existence of anti-correlation between the ionization parameter and metallicity can interpret the presence of anti-correlation between Σ_{SFR} and metallicity.

3.4. The Relation Between Ratio of O32, Σ_* and Σ_{SFR}

We now demonstrate the correlation between the ionization parameter, Σ_* , and Σ_{SFR} . In Figure 5, the different colors represent the bins in different ranges of local stellar mass surface density. The connected lines indicate the median values of the ratio of O32 and Σ_{SFR} in each bin of Σ_* .

The Σ_{SFR} weakly increases with increasing O32, while at the fixed ionization parameter, the regions with higher Σ_*

have higher Σ_{SFR} simultaneously. We find a weak positive correlation between the O32, Σ_* , and Σ_{SFR} relation, which is in agreement with Kewley et al. (2015). We support the scenario that, a more significant number of stars within H II regions, are probably to be mainly accountable for varying the ionization parameter with stellar mass surface density.

3.5. The Fundamental Metallicity Relation

As we mentioned in Figure 2, the $\Sigma_* - Z$ as a function of Σ_{SFR} , for the upper left and right panels, we demonstrate a clear trend with these two metallicity indicators. Here in this section, we suppose to check the secondary relation of Σ_{SFR} . Mannucci et al. (2010) present the existence of the FMR, who estimated the scatter by adopting median metallicity values on the projection MZR space. The projection is described as :

$$\mu_\alpha = \log(\Sigma_*) - \alpha \log(\Sigma_{\text{SFR}}). \quad (8)$$

Interestingly, except at lower stellar mass and higher specific star formation rate, Barrera-Ballesteros et al. (2016) presented that the relationship of $\Sigma_* - Z$ is broadly independent on the total stellar mass of galaxy and specific star formation rate, using O3N2 metallicity calibrator. Before applying FMR projection relation, we excluded the galaxies with lower stellar mass, by setting $\log(M_*/M_\odot) > 9.6$, and we use $\alpha = 0.32$ as proposed by Mannucci et al. (2010) to reduce the scatter of our sample.

In Figure 6, we display the local metallicity distribution as a function of FMR projection μ_α , consistent with Mannucci et al. (2010). We find the scatters of our MaNGA sample are $\sigma = 0.28$ dex and 0.26 dex using metallicity calibrations of N2 and O3N2, respectively. We confirm the existence of the trend in Figure. 2 that regions with higher Σ_{SFR} have lower metallicity at fixed Σ_* . However, the α might not be fitted for the lower Σ_{SFR} region (black lines in Figure 6).

4. DISCUSSION

In this study, we demonstrate the local $\Sigma_* - Z$ relation and their dependence on the Σ_{SFR} and ionization parameter using different metallicity calibrations for spatially resolved samples about 740,000 spaxels from MaNGA survey.

We confirm the tight $\Sigma_* - Z$ relation reported by Rosales-Ortega et al. (2012) and Barrera-Ballesteros et al. (2016). Furthermore, we explore the effect of Σ_{SFR} on the local surface mass density and local metallicity relation or the fundamental relation. We found a clear correlation between $\Sigma_* - Z$, and Σ_{SFR} for the metallicity calibration N2 and O3N2 indexes. Our results in Figure 2 is consistent with global and local FMR studies (e.g., Lara-López et al. 2010; Mannucci et al. 2010; Salim et al. 2014; Sánchez et al. 2013, 2017, 2019) only with N2 and O3N2 metallicity calibrations.

4.1. Physical Explanation of O32 Ratio and Local Metallicity

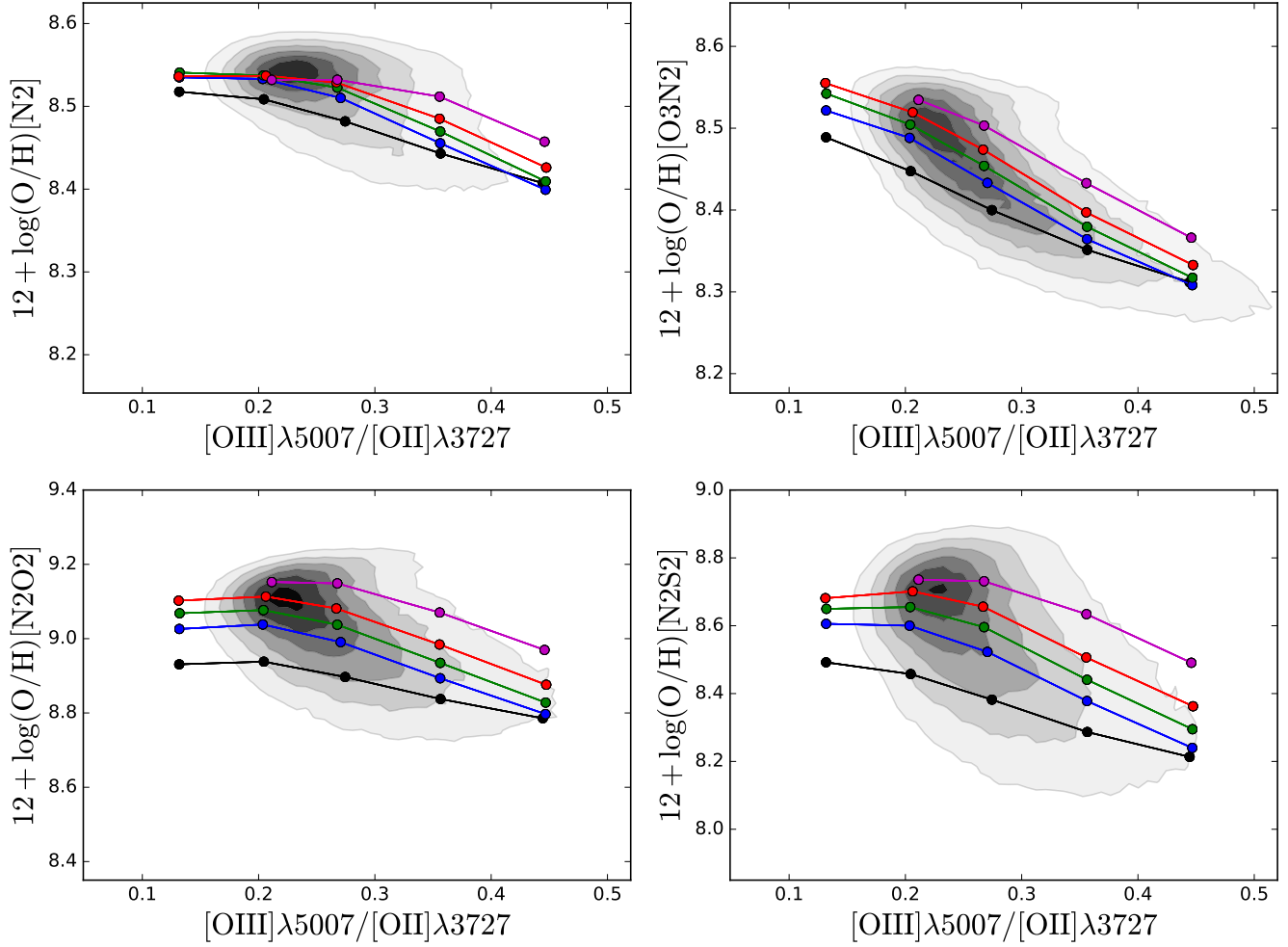


Figure 4. The median metallicity computed with four different metallicity calibrations, O3N2, N2, N2O2, and N2S2 index as a function of the O32 ratio. We separate our spatially resolved MaNGA samples based on local star formation surface density (Σ_{SFR}) in five subsamples. The color-code and symbols are same as Figure 2.

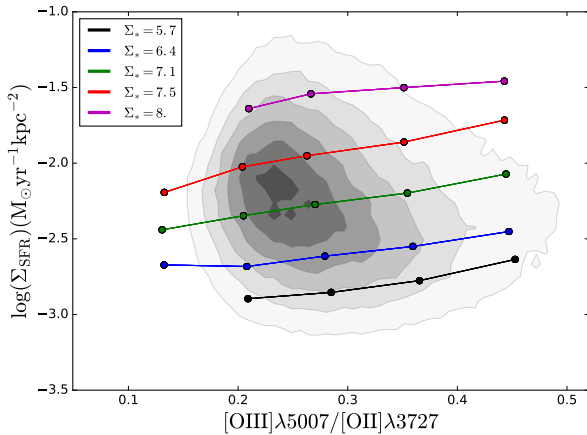


Figure 5. The relation of O32 versus local star formation rate surface density as function of local stellar mass surface density. The different colors indicate the bins of local stellar mass surface density range ($\log(\Sigma_*)$: 5.7, 6.4, 7.1, 7.5 and 8.)

The metallicity anti-correlates with the ratio of O32, which causes the discrepancy with empirical emission lines. [Ho et al. \(2015\)](#) presented the comparison of different diagnosis, and found that the diagnosis of O3N2 offers higher metallicity than the N2O2 at a higher ionization parameter or vice-versa.

The ionization parameter and O32 ratio commonly demonstrate dependence on metallicity since the ionizing spectrum related to metallicity ([Kewley & Dopita 2002](#)). Although low-metallicity stars generate higher ionizing photons and have a harder ionizing spectrum ([Leitherer et al. 2014](#)) as that of an anti-correlation with metallicity and ionization parameter. With these caveats in mind, we present the evidence of the anti-correlation of the metallicity and O32, as shown in Figure 4. Furthermore, [Sanders et al. \(2016\)](#) found that the hardness of the ionizing spectrum increases with decreasing metallicity and higher metallicity objects to have lower O32, lower metallicity tends to higher O32 values.

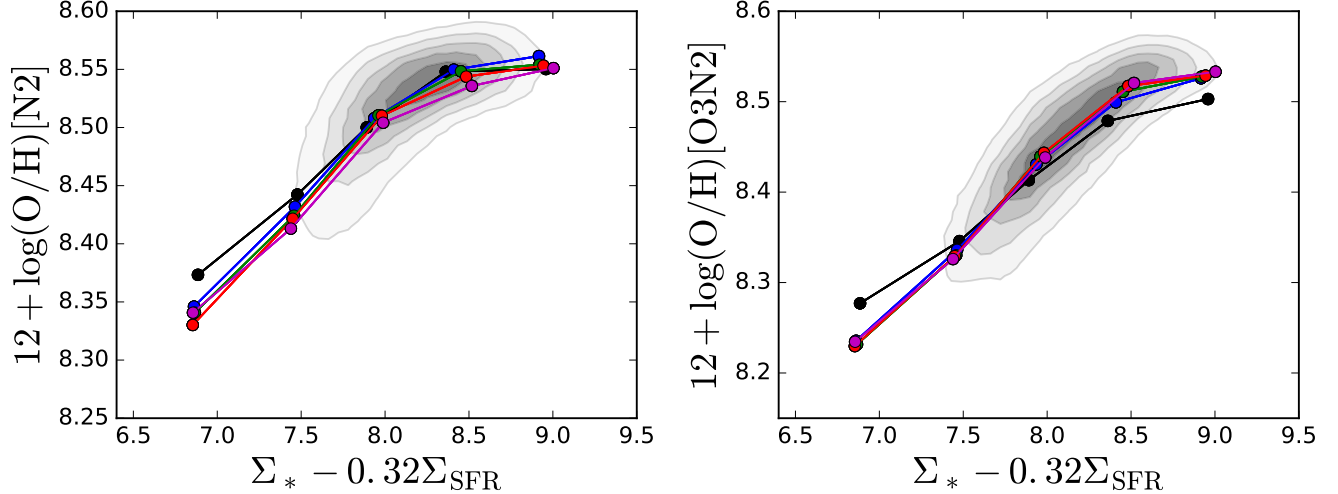


Figure 6. The local metallicity distribution as a function of FMR projection μ_α . The connected color coded lines and gray contour are same as Figure 2. The left and right panels represent FMR for O3N2 and N2 metallicity calibrators.

In other word, as we examine the lower/higher ionization parameter may vary because of the fluctuating the hardness of the ionizing spectrum with metallicity. Regarding this, Nagao et al. (2006) proposed two possibilities, the first one is due to mass-metallicity and mass-age relations. According to this, more massive and older systems are linked with a higher metallicity of galaxies. Due to the decreased luminosity of the ionizing stars, H II regions ionized by later stellar populations are supposed to be distinguished by lower ionization parameters. The other possibility is, the relationship between gas metallicity and stellar metallicity, because lower metallicity stars ionize lower metallicity gas. The first possibility can be checked by the O32 ratio with Σ_{SFR} as shown in Figure 5. Indeed, this related to at a fixed mass surface density, there is an increasing ionization parameter with Σ_{SFR} , this may appear due to the fraction of young stars to old stars in a galaxy.

In addition, as we have seen in Figure 2, the results of different metallicity calibrations agree with suggestions of Curti et al. (2017) and Curti et al. (2019), they found the T_e method metallicity calibration have lower metallicity value than photoionization model calibrations. Indeed, this indicates the higher values of N2O2 and N2S2 are reasonable compared to N2 and O3N2 calibrations. The main reason is that this difference might be caused by the bias at the higher excitation conditions.

4.2. The FMR and $\Sigma_{\text{SFR}} - Z$

Using the metallicity calibration N2 and O3N2, there is an anti-correlation between metallicity and Σ_{SFR} , which recover as Mannucci et al. (2010), however, it changes to positive correlation at the high mass when we use N2O2 and N2S2 indexes. During this condition, did the FMR exist?

Yates et al. (2012) presented the FMR projection, while the SFR anti-correlates to metallicity at lower stellar masses, then the relationship inverts to a positive correlation at higher stellar masses. They argued that the inversion is the consequence of gas-rich mergers at higher stellar masses fueling a starburst. Later, Lara-López et al. (2013) found a similar relation at higher mass; it gives the reversal of the FMR, higher SFR exhibits higher metallicity. However, Telford et al. (2016) presented the systematic effects of the secondary dependence of the MZR on SFR and had a comparison with Mannucci et al. (2010), suggested that it is weaker for the secondary relationship.

Results in Figure 3, have shown a mixed scenario of negative and positive correlations. For N2 and O3N2 metallicity calibrations at low and intermediate mass, we found the negative $\Sigma_{\text{SFR}} - Z$, which is consistent with Mannucci et al. (2010), suggesting that the lower mass produces lower metallicity and higher Σ_{SFR} . On the other hand, this analysis supports the original FMR, only if we use N2 and O3N2 indexes. Indeed, Lian et al. (2015) found at fixed stellar mass, the lower metallicity corresponds to a younger stellar population for local Lyman-break analogs (LBAs) galaxies. For the N2O2 and N2S2 metallicity indicators, the result is challengeable to interpret, as we have seen the positive trend for high mass range. This inverted result is possibly caused by the metallicity calibration. In Section 3, we have seen that for higher Σ_* using N2O2 and N2S2, the MZR is increasing for higher Σ_{SFR} , but is flatter for high mass with N2 and O3N2 calibrators.

Looking back to the two bottom panels of Figure 2, the local metallicity increases with increasing local stellar mass surface density but no trend with local SFR. In Figure 3, the

$\Sigma_{\text{SFR}} - Z$ increases with the increasing stellar mass, this indicates that the stellar mass and local stellar mass surface density are physically fundamental to drive the local metallicity in H II regions.

Kashino et al. (2016) reported that for local galaxies at low mass, the median value of metallicity shows flat or constant. They suggest that this result is due to the dominance of the primary production of nitrogen in less massive galaxies. Their finding is in agreement with our results using the metallicity indicators of N2O2 and N2S2 in Figure 3, the $\Sigma_{\text{SFR}} - Z$ relation is constant at the lower mass bins. Furthermore, Kashino et al. (2016) find an anti-correlation between metallicity and SFR in FMR when using Mannucci et al. (2010) metallicity calibration; it retrieves to a positive trend when using Dopita et al. (2016) metallicity calibration. This is similar to our result that the trend is reversed when using N2O2 and N2S2 indexes metallicity calibrations.

More recently, Curti et al. (2019) derived the MZR for a sample of SDSS galaxies with T_e metallicity calibration, they found the turnover mass and the saturation metallicity are in agreement with previous MZR studies, while showing significantly lower normalization compared to those based on photoionization models. This determination is similar to our result as showing in Figure 2 and 3. Cresci et al. (2019) also reanalyzed the data of CALIFA and SDSS-IV MaNGA samples, and found the secondary relation between MZR and SFR, which are different from the findings in Barrera-Ballesteros et al. (2017) and Sánchez et al. (2017). Cresci et al. (2019) demonstrated that at fixed mass the metallicity depends on SFR, and shows an inversion at high stellar mass region caused by the metallicity calibration and SFR estimation, which is similar to our result.

In conclusion of this section, the different metallicity calibrations give different correlations between the mass surface density, metallicity and local star formation surface density (in Figures 2 and 3). These results may be caused by metallicity calibration, the Σ_{SFR} determination, and the ionization parameter. In general, the electronic temperature method, derived with the ratios of faint auroral to nebular emission lines (e.g., $[\text{O III}]\lambda 4363/[\text{O III}]\lambda 5007$), is regarded as the most reliable approach for the metallicity estimation. However, it is not suitable for spectrum with no such an auroral line detection. To estimate the metallicity with these spectra, O3N2 and N2 diagnosis are calibrated by empirical fitting to the electronic temperature metallicity with emission line ratios (Pettini & Pagel 2004), while the N2O2 and N2S2 diagnosis are based on the photoionization models for H II regions (Kewley & Dopita 2002; Dopita et al. 2016). Because of the different approaches in the calibration, a large discrepancy is found between the metallicities derived by different calibrators (Morisset et al. 2016). For example, the O3N2 and N2 diagnosis can not accurately reproduce the superso-

lar metallicity, the N2O2 and N2S2 calibrators are model-dependent and then provide some uncertainty. As we investigate in Figure 4, we can see the strong correlation between the ratio of O32 and the local metallicity, this is known as the ionization parameter is sensitive to oxygen abundance. Determination of metallicity using strong emission lines may bias the ionization parameter, and it is necessary to find the accurate oxygen abundance. Due to this, there is a correlation between metallicity and local star formation rate surface density. Our result is partly consistent with reported negative correlation between metallicity and SFR (Mannucci et al. 2010; Andrews & Martini 2013), and the positive correlation in Kashino et al. (2016) at the higher mass bins.

5. SUMMARY

This work aims to explore the dependence of local $\Sigma_* - Z - \Sigma_{\text{SFR}}$ relation using the 740,000 spaxels from the MaNGA survey. We try to demonstrate if the local Σ_{SFR} exists or not in FMR. Here, we summarize our findings as follows.

- We present local $\Sigma_* - Z - \Sigma_{\text{SFR}}$ relation using metallicity calibration of O3N2, N2, and N2O2 and N2S2. We find a strong correlation with local Σ_{SFR} using O3N2, N2, but the trend is not obvious with N2O2 and N2S2. This means that the existence of FMR probably depends on the metallicity calibrators.
- We find a mixed relation of $\Sigma_{\text{SFR}} - Z$ (anti-correlation/positive correlation) at lower/higher stellar mass bins according to metallicity derivation. In particular, when using the metallicity from N2O2 and N2S2 indexes, the existence of FMR vanishes at higher masses, while the correlation retrieves using a similar metallicity scale with Mannucci et al. (2010).
- We confirm the dependence of the ratio of O32 on metallicity, which means that a higher ionization parameter is found at lower metallicity, and the lower ionization parameter tends to higher metallicity.
- We provide the FMR after exclusion of low stellar mass, which is a projection of local stellar mass surface density, metallicity, and star formation rate surface density, and find that the scatters are reduced when using N2 and O3N2 indexes, comparing to the $\Sigma_* - Z$ relation.

ACKNOWLEDGMENTS

This work is supported by the National Key R&D Program of China (2017YFA0402600), the B-type Strategic Priority Program of the Chinese Academy of Sciences (XDB41000000) and the National Natural Science Foundation of China (NSFC, Nos. 11421303, and 11973038). Berzaf B. acknowledges support from CAS-TWAS President's Fellowship. We thank Enci Wang for useful discussion. Y.L.G. gratefully acknowledges support from the China Scholarship Council (No. 201906340095).

Funding for the Sloan Digital Sky Survey IV has been provided by the Alfred P. Sloan Foundation, the U.S. Department of Energy Office of Science, and the Participating Institutions. SDSS-IV acknowledges support and resources from the Center for High-Performance Computing at the University of Utah. The SDSS web site is www.sdss.org. SDSS-IV is managed by the Astrophysical Research Consortium for the Participating Institutions of the SDSS Collaboration including the Brazilian Participation Group, the Carnegie Institution for Science, Carnegie Mellon Univer-

sity, the Chilean Participation Group, the French Participation Group, Harvard-Smithsonian Center for Astrophysics, Instituto de Astrofísica de Canarias, The Johns Hopkins University, Kavli Institute for the Physics and Mathematics of the Universe (IPMU)/University of Tokyo, Lawrence Berkeley National Laboratory, Leibniz Institut für Astrophysik Potsdam (AIP), Max-Planck-Institut für Astronomie (MPIA Heidelberg), Max-Planck-Institut für Astrophysik (MPA Garching), Max-Planck-Institut für Extraterrestrische Physik (MPE), National Astronomical Observatory of China, New Mexico State University, New York University, University of Notre Dame, Observatorio Nacional/MCTI, The Ohio State University, Pennsylvania State University, Shanghai Astronomical Observatory, United Kingdom Participation Group, Universidad Nacional Autónoma de México, University of Arizona, University of Colorado Boulder, University of Oxford, University of Portsmouth, University of Utah, University of Virginia, University of Washington, University of Wisconsin, Vanderbilt University, and Yale University.

REFERENCES

- Abolfathi, B., Aguado, D. S., Aguilar, G., et al. 2018, *ApJS*, 235, 42, doi: [10.3847/1538-4365/aa9e8a](https://doi.org/10.3847/1538-4365/aa9e8a)
- Allain, D., Collin-Souffrin, S., Joly, M., & Vigroux, L. 1979, *A&A*, 78, 200
- Andrews, B. H., & Martini, P. 2013, *ApJ*, 765, 140, doi: [10.1088/0004-637X/765/2/140](https://doi.org/10.1088/0004-637X/765/2/140)
- Baldwin, A., Phillips, M. M., & Terlevich, R. 1981, *PASP*, 93, 817, doi: [10.1086/130930](https://doi.org/10.1086/130930)
- Barrera-Ballesteros, J. K., Sánchez, S. F., Heckman, T., Blanc, G. A., & Team, T. M. 2017, *ApJ*, 844, 80, doi: [10.3847/1538-4357/aa7aa9](https://doi.org/10.3847/1538-4357/aa7aa9)
- Barrera-Ballesteros, J. K., Heckman, T. M., Zhu, G. B., et al. 2016, *MNRAS*, 463, 2513, doi: [10.1093/mnras/stw1984](https://doi.org/10.1093/mnras/stw1984)
- Belfiore, F., Maiolino, R., & Bothwell, M. 2016, *MNRAS*, 455, 1218, doi: [10.1093/mnras/stv2332](https://doi.org/10.1093/mnras/stv2332)
- Blanton, M. R., Kazin, E., Muna, D., Weaver, B. A., & Price-Whelan, A. 2011, *AJ*, 142, 31, doi: [10.1088/0004-6256/142/1/31](https://doi.org/10.1088/0004-6256/142/1/31)
- Blanton, M. R., Schlegel, D. J., Strauss, M. A., et al. 2005, *AJ*, 129, 2562, doi: [10.1086/429803](https://doi.org/10.1086/429803)
- Bruzual, G., & Charlot, S. 2003, *MNRAS*, 344, 1000, doi: [10.1046/j.1365-8711.2003.06897.x](https://doi.org/10.1046/j.1365-8711.2003.06897.x)
- Bundy, K., Bershady, M. A., Law, D. R., et al. 2015, *ApJ*, 798, 7, doi: [10.1088/0004-637X/798/1/7](https://doi.org/10.1088/0004-637X/798/1/7)
- Calzetti, D., Armus, L., Bohlin, R. C., et al. 2000, *ApJ*, 533, 682, doi: [10.1086/308692](https://doi.org/10.1086/308692)
- Chabrier, G. 2003, *PASP*, 115, 763, doi: [10.1086/376392](https://doi.org/10.1086/376392)
- Cid Fernandes, R., Mateus, A., Sodré, L., Stasińska, G., & Gomes, J. M. 2005, *MNRAS*, 358, 363, doi: [10.1111/j.1365-2966.2005.08752.x](https://doi.org/10.1111/j.1365-2966.2005.08752.x)
- Cresci, G., Mannucci, F., & Curti, M. 2019, *A&A*, 627, A42, doi: [10.1051/0004-6361/201834637](https://doi.org/10.1051/0004-6361/201834637)
- Curti, M., Cresci, G., Mannucci, F., et al. 2017, *MNRAS*, 465, 1384, doi: [10.1093/mnras/stw2766](https://doi.org/10.1093/mnras/stw2766)
- Curti, M., Mannucci, F., Cresci, G., & Maiolino, R. 2019, *Monthly Notices of the Royal Astronomical Society*, 491, 944
- Dopita, M. A., Kewley, L. J., Heisler, C. A., & Sutherland, R. S. 2000, *ApJ*, 542, 224, doi: [10.1086/309538](https://doi.org/10.1086/309538)
- Dopita, M. A., Kewley, L. J., Sutherland, R. S., & Nicholls, D. C. 2016, *Ap&SS*, 361, 61, doi: [10.1007/s10509-016-2657-8](https://doi.org/10.1007/s10509-016-2657-8)
- Dopita, M. A., Fischera, J., Sutherland, R. S., et al. 2006, *ApJ*, 647, 244, doi: [10.1086/505418](https://doi.org/10.1086/505418)
- Drory, N., MacDonald, N., Bershady, M. A., et al. 2015, *AJ*, 149, 77, doi: [10.1088/0004-6256/149/2/77](https://doi.org/10.1088/0004-6256/149/2/77)
- Ellison, S. L., Patton, D. R., Simard, L., & McConnachie, A. W. 2008, *ApJL*, 672, L107, doi: [10.1086/527296](https://doi.org/10.1086/527296)
- Finlator, K., & Davé, R. 2008, *MNRAS*, 385, 2181, doi: [10.1111/j.1365-2966.2008.12991.x](https://doi.org/10.1111/j.1365-2966.2008.12991.x)
- Gao, Y., Wang, E., Kong, X., et al. 2018, *ApJ*, 868, 89, doi: [10.3847/1538-4357/aae9f1](https://doi.org/10.3847/1538-4357/aae9f1)
- Ho, I.-T., Kudritzki, R.-P., Kewley, L. J., et al. 2015, *MNRAS*, 448, 2030, doi: [10.1093/mnras/stv067](https://doi.org/10.1093/mnras/stv067)
- Hunt, L., Magrini, L., Galli, D., et al. 2012, *MNRAS*, 427, 906, doi: [10.1111/j.1365-2966.2012.21761.x](https://doi.org/10.1111/j.1365-2966.2012.21761.x)

- Kaasinen, M., Kewley, L., Bian, F., et al. 2018, *MNRAS*, 477, 5568, doi: [10.1093/mnras/sty1012](https://doi.org/10.1093/mnras/sty1012)
- Kashino, D., Renzini, A., Silverman, J. D., & Daddi, E. 2016, *ApJL*, 823, L24, doi: [10.3847/2041-8205/823/2/L24](https://doi.org/10.3847/2041-8205/823/2/L24)
- Kauffmann, G., Heckman, T. M., White, S. D. M., et al. 2003, *MNRAS*, 341, 33, doi: [10.1046/j.1365-8711.2003.06291.x](https://doi.org/10.1046/j.1365-8711.2003.06291.x)
- Kennicutt, Jr., R. C. 1998, *ARA&A*, 36, 189, doi: [10.1146/annurev.astro.36.1.189](https://doi.org/10.1146/annurev.astro.36.1.189)
- Kewley, L. J., & Dopita, M. A. 2002, *ApJS*, 142, 35, doi: [10.1086/341326](https://doi.org/10.1086/341326)
- Kewley, L. J., Dopita, M. A., Leitherer, C., et al. 2013, *ApJ*, 774, 100, doi: [10.1088/0004-637X/774/2/100](https://doi.org/10.1088/0004-637X/774/2/100)
- Kewley, L. J., Dopita, M. A., Sutherland, R. S., Heisler, C. A., & Trevena, J. 2001, *ApJ*, 556, 121, doi: [10.1086/321545](https://doi.org/10.1086/321545)
- Kewley, L. J., & Ellison, S. L. 2008, *ApJ*, 681, 1183, doi: [10.1086/587500](https://doi.org/10.1086/587500)
- Kewley, L. J., Zahid, H. J., Geller, M. J., et al. 2015, *ApJL*, 812, L20, doi: [10.1088/2041-8205/812/2/L20](https://doi.org/10.1088/2041-8205/812/2/L20)
- Lara-López, M. A., López-Sánchez, Á. R., & Hopkins, A. M. 2013, *ApJ*, 764, 178, doi: [10.1088/0004-637X/764/2/178](https://doi.org/10.1088/0004-637X/764/2/178)
- Lara-López, M. A., Cepa, J., Bongiovanni, A., et al. 2010, *A&A*, 521, L53, doi: [10.1051/0004-6361/201014803](https://doi.org/10.1051/0004-6361/201014803)
- Leitherer, C., Ekström, S., Meynet, G., et al. 2014, *ApJS*, 212, 14, doi: [10.1088/0067-0049/212/1/14](https://doi.org/10.1088/0067-0049/212/1/14)
- Lequeux, J., Peimbert, M., Rayo, J. F., Serrano, A., & Torres-Peimbert, S. 1979, *A&A*, 80, 155
- Li, C., Wang, E., Lin, L., et al. 2015, *ApJ*, 804, 125, doi: [10.1088/0004-637X/804/2/125](https://doi.org/10.1088/0004-637X/804/2/125)
- Lian, J. H., Li, J. R., Yan, W., & Kong, X. 2015, *MNRAS*, 446, 1449, doi: [10.1093/mnras/stu2184](https://doi.org/10.1093/mnras/stu2184)
- Lilly, S. J., Carollo, C. M., Pipino, A., Renzini, A., & Peng, Y. 2013, *ApJ*, 772, 119, doi: [10.1088/0004-637X/772/2/119](https://doi.org/10.1088/0004-637X/772/2/119)
- Ly, C., Malkan, M. A., Nagao, T., et al. 2014, *ApJ*, 780, 122, doi: [10.1088/0004-637X/780/2/122](https://doi.org/10.1088/0004-637X/780/2/122)
- Maier, C., Meisenheimer, K., & Hippelein, H. 2004, *A&A*, 418, 475, doi: [10.1051/0004-6361:20035795](https://doi.org/10.1051/0004-6361:20035795)
- Mannucci, F., Cresci, G., Maiolino, R., Marconi, A., & Gnerucci, A. 2010, *MNRAS*, 408, 2115, doi: [10.1111/j.1365-2966.2010.17291.x](https://doi.org/10.1111/j.1365-2966.2010.17291.x)
- Marino, R. A., Rosales-Ortega, F. F., Sánchez, S. F., et al. 2013, *A&A*, 559, A114, doi: [10.1051/0004-6361/201321956](https://doi.org/10.1051/0004-6361/201321956)
- Markwardt, C. B., Swank, J. H., Barthelmy, S. D., et al. 2009, *The Astronomer's Telegram*, 2258
- Moran, S. M., Heckman, T. M., Kauffmann, G., et al. 2012, *ApJ*, 745, 66, doi: [10.1088/0004-637X/745/1/66](https://doi.org/10.1088/0004-637X/745/1/66)
- Morisset, C., Delgado-Inglada, G., Sánchez, S. F., et al. 2016, *A&A*, 594, A37, doi: [10.1051/0004-6361/201628559](https://doi.org/10.1051/0004-6361/201628559)
- Nagao, T., Maiolino, R., & Marconi, A. 2006, *A&A*, 459, 85, doi: [10.1051/0004-6361:20065216](https://doi.org/10.1051/0004-6361:20065216)
- Nakajima, K., & Ouchi, M. 2014, *MNRAS*, 442, 900, doi: [10.1093/mnras/stu902](https://doi.org/10.1093/mnras/stu902)
- Pettini, M., & Pagel, B. E. J. 2004, *MNRAS*, 348, L59, doi: [10.1111/j.1365-2966.2004.07591.x](https://doi.org/10.1111/j.1365-2966.2004.07591.x)
- Raimann, D., Storchi-Bergmann, T., Bica, E., Melnick, J., & Schmitt, H. 2000, *MNRAS*, 316, 559, doi: [10.1046/j.1365-8711.2000.03526.x](https://doi.org/10.1046/j.1365-8711.2000.03526.x)
- Rosales-Ortega, F. F., Sánchez, S. F., Iglesias-Páramo, J., et al. 2012, *ApJL*, 756, L31, doi: [10.1088/2041-8205/756/2/L31](https://doi.org/10.1088/2041-8205/756/2/L31)
- Saintonge, A., Kauffmann, G., Kramer, C., et al. 2011, *MNRAS*, 415, 32, doi: [10.1111/j.1365-2966.2011.18677.x](https://doi.org/10.1111/j.1365-2966.2011.18677.x)
- Salim, S., Lee, J. C., Ly, C., et al. 2014, *ApJ*, 797, 126, doi: [10.1088/0004-637X/797/2/126](https://doi.org/10.1088/0004-637X/797/2/126)
- Sánchez, S. F., Kennicutt, R. C., Gil de Paz, A., et al. 2012, *A&A*, 538, A8, doi: [10.1051/0004-6361/201117353](https://doi.org/10.1051/0004-6361/201117353)
- Sánchez, S. F., Rosales-Ortega, F. F., Jungwiert, B., et al. 2013, *A&A*, 554, A58, doi: [10.1051/0004-6361/201220669](https://doi.org/10.1051/0004-6361/201220669)
- Sánchez, S. F., Barrera-Ballesteros, J. K., Sánchez-Menguiano, L., et al. 2017, *MNRAS*, 469, 2121, doi: [10.1093/mnras/stx808](https://doi.org/10.1093/mnras/stx808)
- Sánchez, S. F., Barrera-Ballesteros, J. K., López-Cobá, C., et al. 2019, *MNRAS*, 484, 3042, doi: [10.1093/mnras/stz019](https://doi.org/10.1093/mnras/stz019)
- Sánchez Almeida, J., Caon, N., Muñoz-Tuñón, C., Filho, M., & Cerviño, M. 2018, *MNRAS*, 476, 4765, doi: [10.1093/mnras/sty510](https://doi.org/10.1093/mnras/sty510)
- Sánchez Almeida, J., & Sánchez-Menguiano, L. 2019, *ApJL*, 878, L6, doi: [10.3847/2041-8213/ab218d](https://doi.org/10.3847/2041-8213/ab218d)
- Sanders, R. L., Shapley, A. E., Kriek, M., et al. 2016, *ApJ*, 816, 23, doi: [10.3847/0004-637X/816/1/23](https://doi.org/10.3847/0004-637X/816/1/23)
- Schlegel, D. J., Finkbeiner, D. P., & Davis, M. 1998, *ApJ*, 500, 525, doi: [10.1086/305772](https://doi.org/10.1086/305772)
- Storchi-Bergmann, T., Calzetti, D., & Kinney, A. L. 1994, *ApJ*, 429, 572, doi: [10.1086/174345](https://doi.org/10.1086/174345)
- Telford, O. G., Dalcanton, J. J., Skillman, E. D., & Conroy, C. 2016, *ApJ*, 827, 35, doi: [10.3847/0004-637X/827/1/35](https://doi.org/10.3847/0004-637X/827/1/35)
- Tremonti, C. A., Heckman, T. M., Kauffmann, G., et al. 2004, *ApJ*, 613, 898, doi: [10.1086/423264](https://doi.org/10.1086/423264)
- Wu, Y.-Z., Zhang, S.-N., Zhao, Y.-H., & Zhang, W. 2016, *MNRAS*, 457, 2929, doi: [10.1093/mnras/stw113](https://doi.org/10.1093/mnras/stw113)
- Yates, R. M., Kauffmann, G., & Guo, Q. 2012, *MNRAS*, 422, 215, doi: [10.1111/j.1365-2966.2012.20595.x](https://doi.org/10.1111/j.1365-2966.2012.20595.x)
- Zahid, H. J., Kashino, D., Silverman, J. D., et al. 2014, *ApJ*, 792, 75, doi: [10.1088/0004-637X/792/1/75](https://doi.org/10.1088/0004-637X/792/1/75)